PROGRESS IN AEROSPACE AND AVIATION TECHNOLOGY
e-ISSN: 2821-2924

PAAT

Vol. 5 No. 1 (2025) 41-54
https://publisher.uthm.edu.my/ojs/index.php/paat

Aerodynamic Study of a Two Groove on the Upper Surface of an Airfoil at Low Angles of Attack

Esmail Abdullah[1], Mohd Fauzi Yaakub[1]*, Muhammad Aideed Azman[1], Wan Muhammad Aqil Wan Nawang[1]

[1] *Research Center for Unmanned Vehicle (RECUV), Faculty of Mechanical and Manufacturing Engineering, Universiti Tun Hussein Onn Malaysia, 86400 Parit Raja, Batu Pahat, Johor, MALAYSIA*

*Corresponding Author: fauziy@uthm.edu.my
DOI: https://doi.org/10.30880/paat.2025.05.01.005

Article Info

Received: 21 February 2025
Accepted: 19 May 2025
Available online: 30 June 2025

Keywords

Angle of Attack, lift, drag, airflow, simulation, aerodynamics, groove

Abstract

This study investigates the aerodynamic effects of introducing two semicircular grooves on the upper surface of a NACA 0012 airfoil at low angles of attack using computational fluid dynamics (CFD). The purpose of this research is to evaluate how groove geometry, depth, and spacing influence the lift and drag characteristics and to determine the optimal groove configuration that enhances aerodynamic performance. ANSYS Fluent was utilized to simulate the airflow over a baseline smooth airfoil and modified versions featuring grooves of varying sizes and positions. A grid independence test was conducted to ensure the accuracy and numerical reliability of the simulation. The baseline airfoil simulation was validated against experimental data, showing good agreement with a maximum relative error of less than 10%. The results revealed that a single groove of 0.01c depth provided an increase in lift and a notable drag reduction, particularly at a 10° angle of attack. Further investigations with two grooves, where the first groove was fixed at 0.25c and the second varied between 0.239c and 0.45c, showed that the optimal configuration was with the second groove placed at 0.35c. The study concludes that proper groove positioning and sizing can effectively delay flow separation, enhance lift, and reduce drag in low-speed aerodynamic applications. These findings suggest potential benefits for UAVs, gliders, and other airfoil-based systems operating at low angles of attack.

1. Introduction

Airfoils, representing the cross-sectional shapes of aircraft wings, helicopter blades, wind turbine blades, and other lifting surfaces, are fundamental to aerodynamic performance. These structures generate lift and drag forces when exposed to airflow, with lift enabling flight and maneuverability, while drag opposes motion and increases fuel consumption. Since the advent of powered flight in the early 20th century, airfoil design has evolved to enhance efficiency, speed, and safety in aviation. Symmetrical airfoils, such as the NACA 0012, are particularly valued in applications requiring balanced performance at low angles of attack, including unmanned aerial vehicles (UAVs), gliders, and small-scale wind tunnels, where maximizing lift while minimizing drag is essential.

Recent research has focused on surface modifications to airfoils, such as textures that induce controlled vortices to energize the boundary layer, delay flow separation, and reduce pressure drag. Flow separation, where the airflow detaches from the airfoil surface, leads to stall, diminished lift, and increased drag, posing risks to performance and safety. By introducing features like dimples or grooves, these modifications promote turbulence, which enhances boundary layer attachment, particularly at higher angles of attack. For instance, Liu et al. [1] demonstrated that surface grooves on a NACA 4415 airfoil eliminate laminar separation bubbles at low Reynolds

numbers, improving aerodynamic efficiency for small wind turbines by reducing drag while maintaining lift. Likewise, Mustak et al. [2] studied different dimple shapes (spherical, hexagonal, cylindrical, and square) on airfoils and found that they help keep the airflow attached longer, allow for higher angles before stalling, and improve the lift-to-drag ratios, although the best shapes depend on the flow conditions.

Chalia and Bharti also worked on a NACA 2412 airfoil by adding spherical dimples and vortex generators, which helped delay stalling and increase lift, but this came with the downside of more drag at some angles. Srivastav explored dimple shapes for flow control, noting reductions in pressure drag through turbulence generation [4]. Livya et al. analyzed dimples on a NACA 0018 airfoil, reporting improved lift and delayed separation at subsonic speeds [5]. Validation of such studies often relies on fundamental experimental data, as provided by Abbott and Von Doenhoff [6], who compiled comprehensive airfoil performance metrics, including lift and drag coefficients for NACA series airfoils.

Correlations between these studies show that surface modifications frequently delay separation and improve lift-to-drag ratios at moderate angles of attack, particularly in low-Reynolds-number flows relevant to UAVs. However, contradictions emerge regarding drag: while pressure drag lowers due to reduced wake formation, viscous drag may increase due to increased turbulence, as highlighted by Liu et al. [1] and Chalia and Bharti [3]. Uncertainty exists in ideal geometry, for example, spherical versus pyramidal features and their sensitivity to Reynolds' number or angle of attack. There are gaps in research, such as not enough studies on different grooves on symmetrical airfoils at low angles of attack, detailed comparisons of groove depth and spacing, and how they work with changing flow conditions.

To address these, the present study employs computational fluid dynamics (CFD) via ANSYS Fluent to simulate airflow over a NACA 0012 airfoil modified with two semicircular grooves on the upper surface. Groove depth, width, and spacing are varied at angles of attack from 0° to 10°, with validation against experimental data from Abbott and Von Doenhoff [6] to ensure accuracy. This approach aims to identify configurations that optimize lift enhancement and drag reduction, bridging gaps in low-speed applications. The results will demonstrate how groove-induced vortices mitigate separation, offering information about pressure distributions, velocity contours, and overall performance improvements, which inform subsequent discussions on practical implications for aircraft design.

2. Methodology

The methodology employed in this study utilizes computational fluid dynamics (CFD) to investigate the aerodynamic effects of two semicircular grooves on the upper surface of a NACA 0012 airfoil. Simulations were conducted using ANSYS Fluent software, focusing on low angles of attack ranging from 0° to 10°. The approach covers model validation, parametric evaluation of groove configurations, and comparison with a baseline smooth airfoil.

2.1 Simulation Setup

The core CFD involved the following processes: geometry design, meshing, boundary condition setup, solver configuration, and simulation runs. The final phase of simulation involves post-processing, encompassing grid independence testing, validation against experimental data [6], computation of lift and drag coefficients, and analysis of flow characteristics like pressure distributions and velocity contours. The airfoil geometry parameters are summarized in Table 1.

Table 1 *The summary of airfoil geometry*

Type of airfoil	NACA0012
Chord length	1m
Angle of attack	0^o, 2^o, 4^o, 6^o, 8^o, 10^o

2.1.1 Design Geometry

The two-dimensional (2D) airfoil profile was generated using coordinate data obtained from Airfoil Tools. Points were connected to form the NACA 0012 shape. A C-shaped fluid domain, measuring 10 times the chord length (10c) in both upstream and downstream directions, was sketched on the XY-plane. A semicircle was incorporated and trimmed to define the far-field boundary. Boolean operations were applied to subtract the airfoil from the domain, creating the computational region. Additional sketch lines were projected to partition the domain into multiple faces, aiding in structured meshing. The airfoil was then rotated to achieve the specified angle of attack for each simulation case (Fig. 1).

Progress in Aerospace and Aviation Technology Vol. 5 No. 1 (2025) p. 41-54

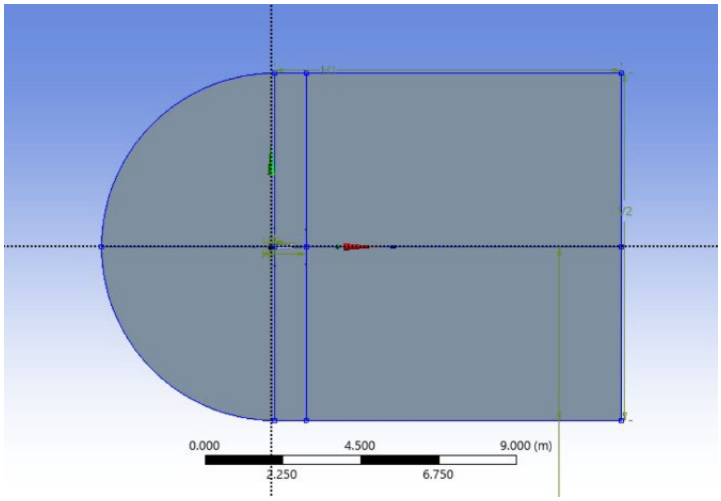

Fig. 1 *Fluid domain of the airfoil*

2.1.2 Meshing

Meshing was performed using sizing and face meshing features for the baseline airfoil. For configurations with grooves, an inflation layer was added to capture boundary layer effects accurately. Edge sizing divided the airfoil into 200 elements to enhance resolution near the surface, where flow gradients are pronounced. All faces were meshed using quadrilateral elements to maintain high-quality structured grids (Fig. 2). This approach ensures numerical stability and minimizes discretization errors, as finer meshing near critical regions improves the accuracy of aerodynamic predictions.

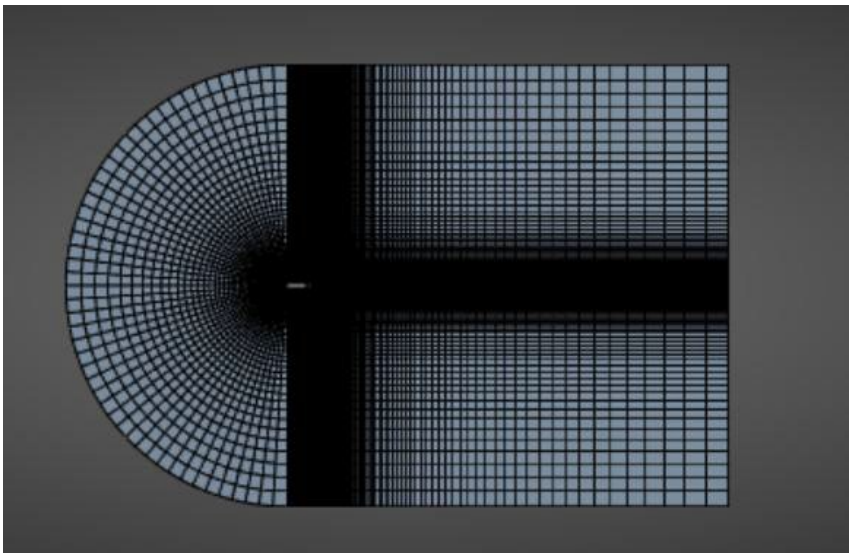

Fig. 2 *The complete meshing of the airfoil*

2.1.3 Boundary Setup

The simulation parameters are detailed in Table 2. The k-ω Shear Stress Transport (SST) turbulence model was selected for its robustness in handling adverse pressure gradients and flow separation, common in airfoil simulations at varying angles of attack.

Table 2 *Parameter setup for the model*

Setup	
Model	K omega
Solver	Density Based
Velocity Formulation	Absolute
Time	Steady
2D space	Planar
Model	
Model	K Omega SST
Material selection	
Air	Density (kg/m^3) = 1.225 Cp (specific heat) = 1006.43 j/kg-k Thermal conductivity = 0.0242 w/m-k Viscosity = 1.789e-5 kg/m-s
Boundary condition	
Free	Type: Pressure far field Gauge Pressure = 0 Mach Number = 0 x-component of flow direction = 1 y-component of flow direction = 0
Inlet	Type: Velocity inlet Velocity Specification Method = Magnitude and direction Reference Frame = Absolute Velocity Magnitude = 43.9 m/s Supersonic/initial gauge pressure = 0 Pa X-component of flow direction = 1 Y-component of flow direction = 0 Turbulence Specification method = Turbulent Viscosity Ratio Turbulent Viscosity Ratio = 1
Outlet	Type: pressure outlet Gauge Pressure = 0 Pa Backflow direction specification Method = Normal to Boundary Turbulence Specification Method: Turbulent Viscosity Ratio Backflow Turbulent Viscosity ratio = 1

Progress in Aerospace and Aviation Technology Vol. 5 No. 1 (2025) p. 41-54

Solution methods and controls are outlined in Table 3, employing a coupled pressure-velocity scheme and second-order upwind discretization for enhanced accuracy. This setup replicates low-speed incompressible flow conditions, with a velocity of 43.9 m/s corresponding to a Reynolds number suitable for UAV applications. Grid independence tests, detailed in the results section, confirmed the mesh resolution's adequacy.

Table 3 *Solution methods*

Solution Method	
Model	K Omega
Pressure velocity coupling	Scheme: coupled
Special discretization	
Gradient	Least squares cell-based
Flow	Second-order upwind
Modified Turbulent viscosity	Second-order upwind
	Solution control
	Courant number: 5
	Under relaxation factor:
	Modified turbulent viscosity = 0.75
	Turbulent viscosity = 1
	Solid = 1
	Monitors
Residual and force monitor	Create: Drag coefficient Wall zones: airfoil Option: Print to console and plot Force vector: X=1, Y=0
	Create: lift coefficient Wall zones: airfoil Option: Print to console and plot Force vector: X=0, Y=1
Solution initialization	
Method	Hybrid initialization
Compute from	Inlet
Ref. frame	Relative to cell zone
Initial values	Gauge pressure (Pa) = 0 X velocity (m/s) = 43.9 Y velocity (m/s) = 0 T(K)=300
Run calculation	
Number of iterations = 500	

3. Results and Discussion

This section presents the outcomes of the CFD simulations conducted on the NACA 0012 airfoil, including grid independence testing, validation against experimental data, and parametric analyses of groove configurations. The results focus on lift coefficient (Cl), drag coefficient (Cd), pressure distributions, and velocity contours at angles of attack (AOA) ranging from 0° to 10°. Discussions interpret the findings in the context of aerodynamic performance, highlighting the effects of groove depth, positioning, and spacing on flow behavior, boundary layer control, and overall efficiency.

3.1 Grid Independence Test

A grid independence test was performed to determine the optimal mesh resolution that yields accurate results independent of further refinement, thereby ensuring computational efficiency and reliability. Simulations for the baseline NACA 0012 airfoil were executed at varying node counts (60450, 92390, and 136730) across the specified AOA range. The lift and drag coefficients were monitored to assess convergence. Fig. 3 illustrates the variation in Cl with AOA for different mesh densities, while Fig. 4 shows the corresponding Cd trends. As the node count increases, the curves converge, with minimal differences observed between the 92,390-node and 136,730-node meshes, indicating that further refinement provides negligible improvements. Table 4 summarizes the Cl and Cd values of the baseline airfoil (NACA0012) at different numbers of nodes. The results demonstrate convergence at approximately 92,390 nodes, where deviations in Cl and Cd are less than 0.5% compared to the finest mesh. This resolution was selected for subsequent simulations to balance accuracy and computational cost.

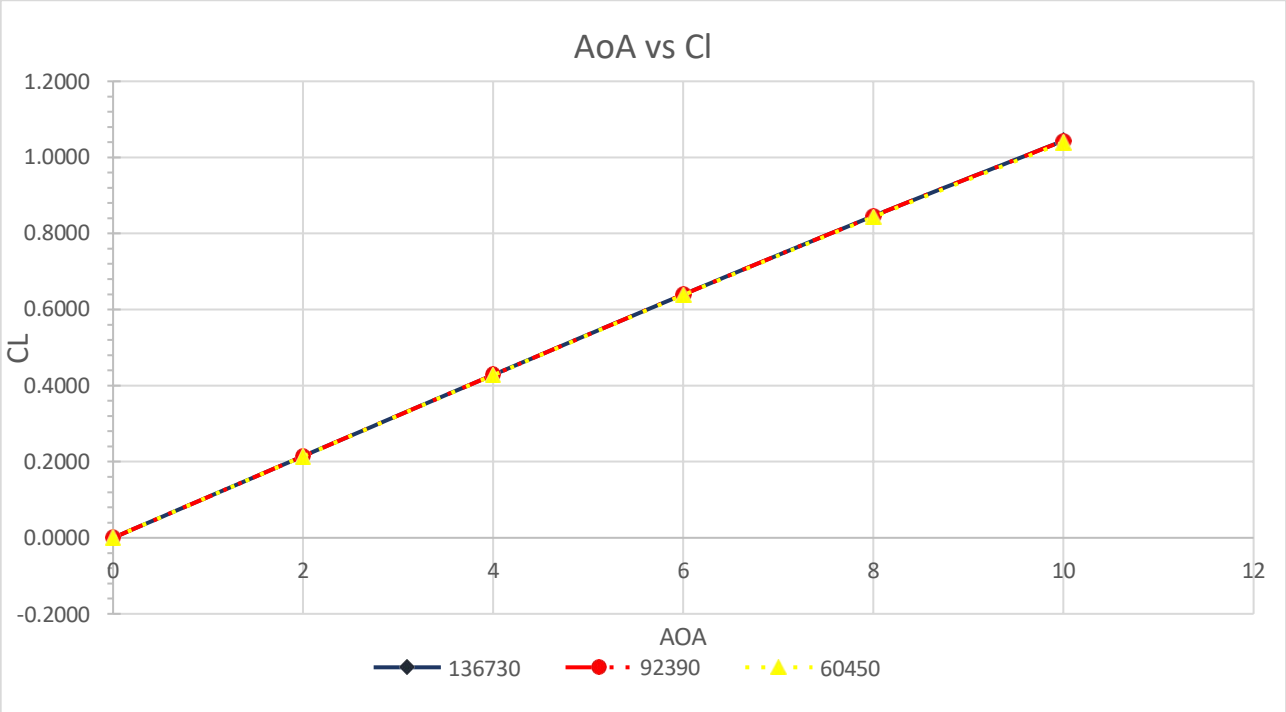

Fig. 3 *Graph of grid independence test for AOA vs. Cl for baseline airfoil*

Progress in Aerospace and Aviation Technology Vol. 5 No. 1 (2025) p. 41-54

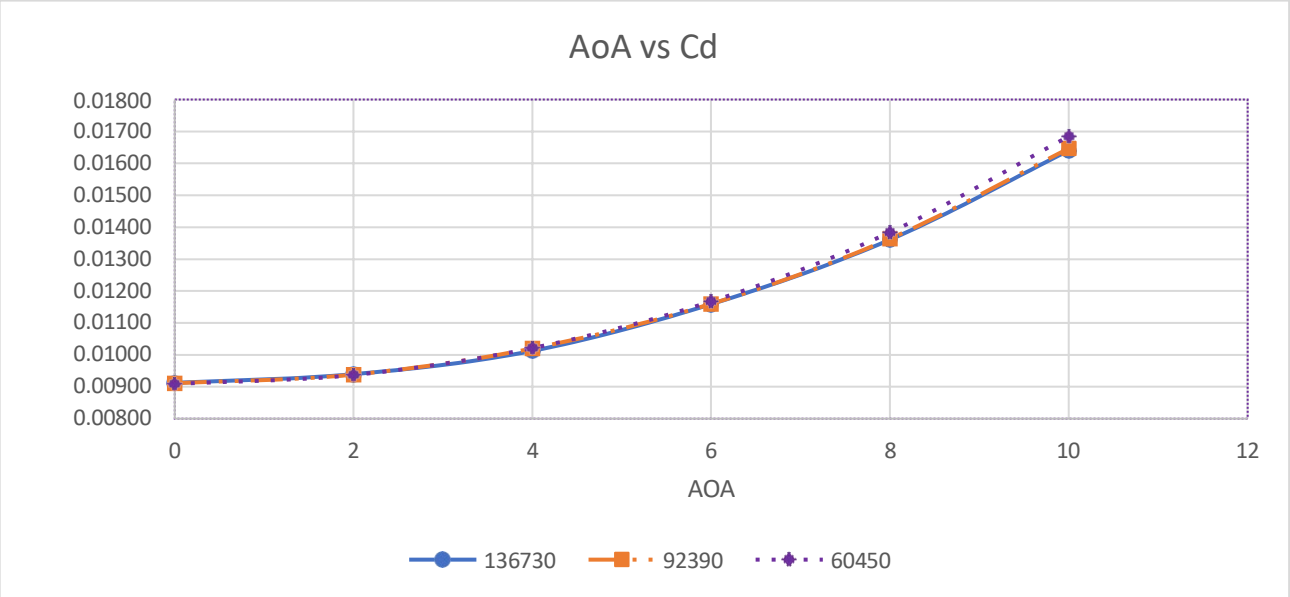

Fig. 4 *Graph of grid independence test for AOA vs. Cd for baseline airfoil*

Table 4 *Cl and Cd of baseline airfoil at different numbers of nodes*

	Lift coefficient (Cl)			Drag coefficient (Cd)		
AOA	**136730**	**92390**	**60450**	**136730**	**92390**	**60450**
0	0.00000	0.00000	0.00000	0.00912	0.00910	0.00909
2	0.21458	0.21450	0.21415	0.00939	0.00938	0.00937
4	0.42830	0.42819	0.42751	0.01012	0.01020	0.01021
6	0.63951	0.63938	0.63808	0.01158	0.01159	0.01167
8	0.84585	0.84565	0.84320	0.01360	0.01364	0.01384
10	1.04400	1.04360	1.03940	0.01640	0.01646	0.01685

To validate the CFD model, simulation results for the baseline airfoil were compared with experimental data from Abbott and Von Doenhoff [6]. Fig. 5 depicts the Cl versus AOA curves for both experimental and simulated cases, showing close alignment across the tested range. Table 5 shows the comparison between experimental and simulation lift coefficient data for various AOAs. The experimental Cl values are generally higher than the simulated ones, with an average error below 3% and a maximum of about 7%. This difference is due to the fact that 2D simulations can't capture three-dimensional effects like spanwise flow or tip vortices that occur in real experiments [6]. Nonetheless, the agreement validates the CFD model's suitability for predicting aerodynamic trends, with errors within acceptable limits for engineering applications (typically <10%).

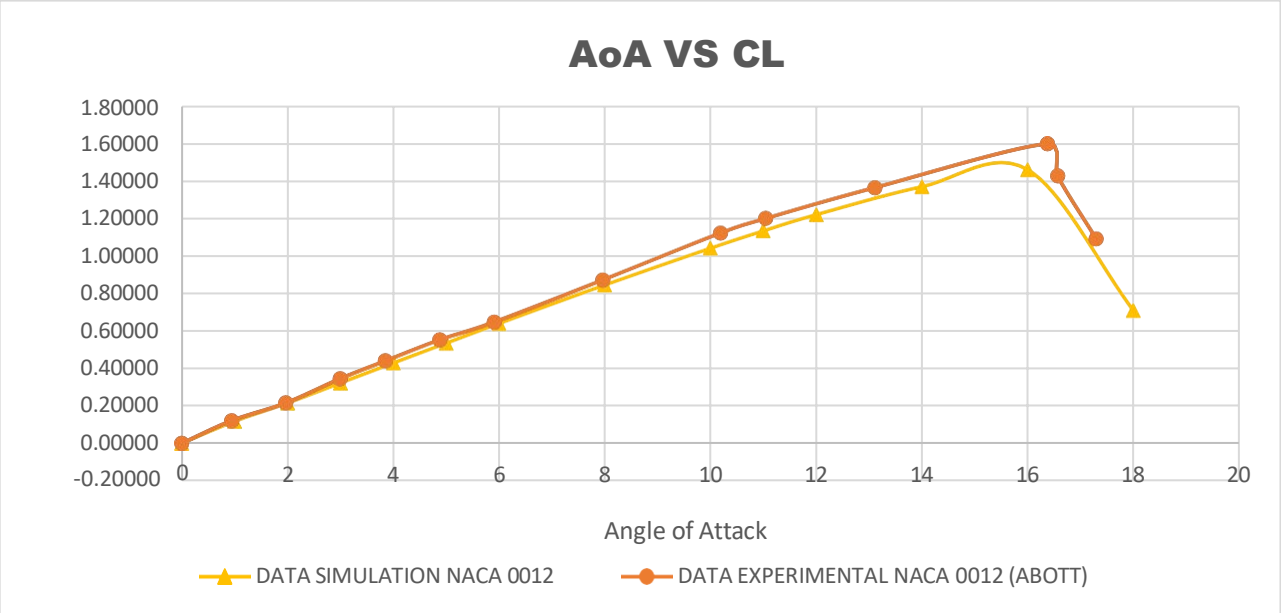

Fig. 5 *Graph AOA vs. CL*

Table 5 *Experimental and simulation lift coefficient*

No.	Angle of Attack (°)	Cl Experimental	CL Simulation	Error	Error Percentage
1	0.00000	0.00000	0.00000	0.00000	0.00%
2	0.94001	0.12061	0.11711	-0.02903	2.90%
3	1.96944	0.21553	0.21415	-0.00641	0.64%
4	2.99515	0.34477	0.32104	-0.06882	6.88%
5	3.85131	0.43960	0.42751	-0.02749	2.75%
6	4.87888	0.55168	0.53330	-0.03332	3.33%
7	5.90831	0.64660	0.63808	-0.01318	1.32%
8	7.96346	0.87076	0.84319	-0.03166	3.17%
9	10.18910	1.12074	1.03937	-0.07261	7.26%
10	11.04710	1.19842	1.13178	-0.05561	5.56%
11	16.56780	1.42443	1.45853	0.02394	2.39%

3.2 Simulation Result of a Semicircular Groove with Different Size

This subsection evaluates the impact of single semicircular groove depths (0.005c, 0.01c, and 0.015c, where c is the chord length) on the airfoil's performance compared to the baseline. Simulations were conducted at the specified AOA range. Fig. 6 presents the Cl versus AOA for each groove depth, while Table 6 provides the corresponding Cl values. The Cl increases with AOA for all configurations. The 0.01c depth yields the highest Cl at moderate AOA, with improvements of up to 3.06% at 0° and sustained gains at higher angles, likely due to enhanced boundary layer energization and delayed separation. The 0.005c depth shows negligible effects, while 0.015c results in slight reductions, particularly at low AOA, suggesting excessive flow disruption.

Progress in Aerospace and Aviation Technology Vol. 5 No. 1 (2025) p. 41-54

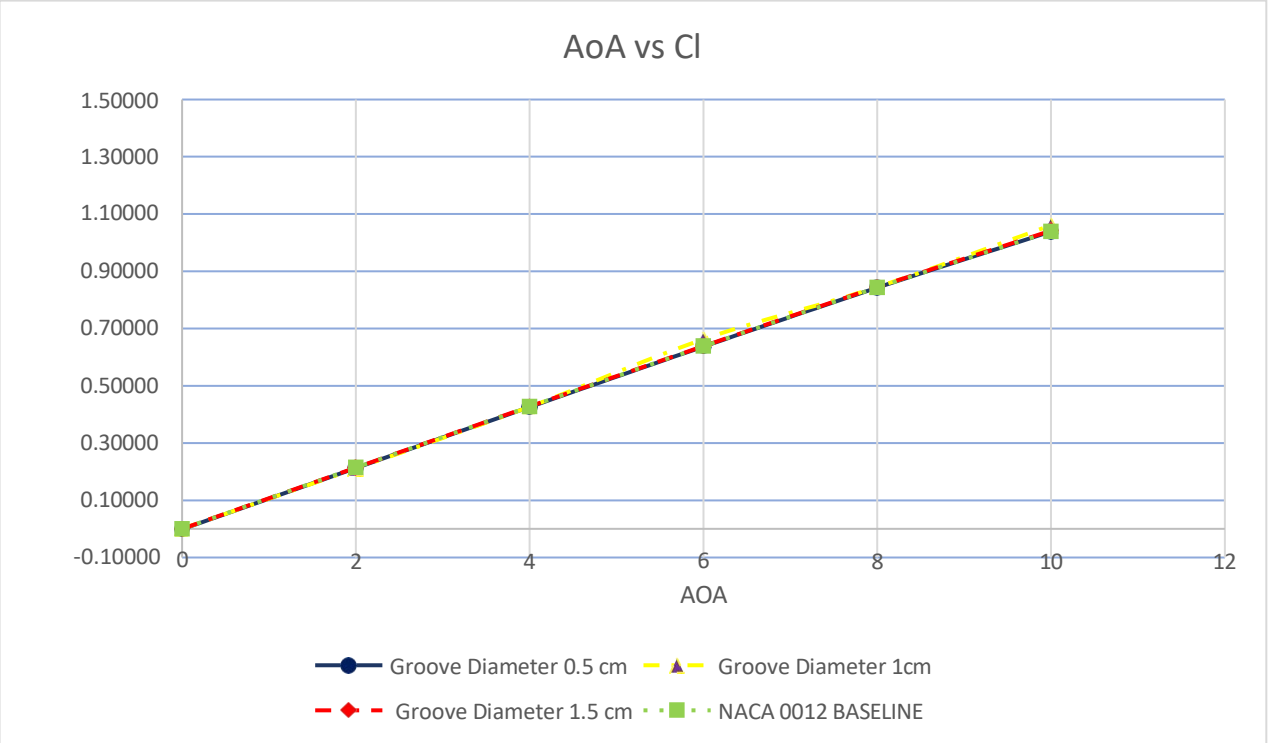

Fig. 6 *Graph angle of attack vs. lift coefficient.*

Table 6 *Lift coefficient of different sizes of grooves*

Lift Coefficient				
D/AOA	0.005c	0.01c	0.015c	baseline
0	-0.00003	0.00022	-0.00116	0.00000
2	0.21373	0.21140	0.21278	0.21415
4	0.42746	0.42690	0.42596	0.42751
6	0.63818	0.66281	0.63706	0.63808
8	0.84450	0.84512	0.84284	0.84319
10	1.04170	1.06077	1.03912	1.03937

Fig. 7 and Table 7 detail the Cd trends for different sizes of grooves. Cd increases with AOA across all cases. The 0.01c depth reduces Cd by up to 8.85% at 10°, indicating effective delay of flow separation. In contrast, 0.015c increases Cd consistently, highlighting a trade-off with deeper grooves. Overall, the 0.01c groove depth optimizes performance by enhancing Cl and reducing Cd, supporting its selection for dual-groove studies. This aligns with prior findings on surface modifications promoting turbulence for better flow attachment [1], [2].

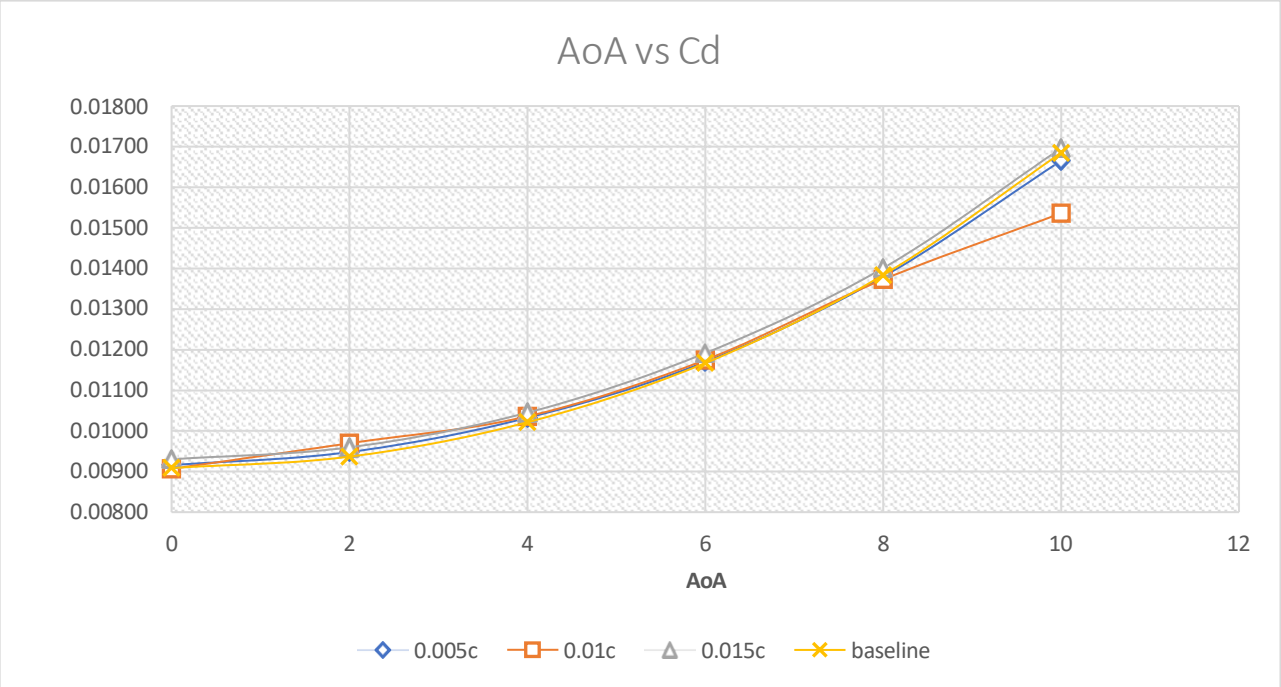

Fig. 7 *Angle of attack vs. drag coefficient*

Table 7 *Drag coefficient of different sizes of grooves*

Drag Coefficient				
D / AOA	0.005c	0.01c	0.015c	baseline
0	0.00916	0.00907	0.00930	0.00909
2	0.00948	0.00970	0.00960	0.00937
4	0.01032	0.01036	0.01045	0.01021
6	0.01170	0.01175	0.01192	0.01167
8	0.01380	0.01373	0.01401	0.01384
10	0.01665	0.01536	0.01696	0.01685

3.3 Simulation Result for Two Grooves with One Groove Fixed at 0.25c

Building on the single-groove results, this analysis examines dual grooves (diameter 0.01c), with one fixed at 0.25c and the second varying at positions 0.239c, 0.261c, 0.30c, 0.35c, 0.40c, and 0.45c. Fig. 1 and Table 8 show Cl variations for different positions of the groove. At 0° AOA, configurations exhibit slightly negative Cl, with the 0.35c position showing the most pronounced effect, potentially due to altered pressure gradients. The 0.35c position enhances Cl most effectively at higher AOA, with gains attributed to synergistic vortex generation between grooves.

Progress in Aerospace and Aviation Technology Vol. 5 No. 1 (2025) p. 41-54

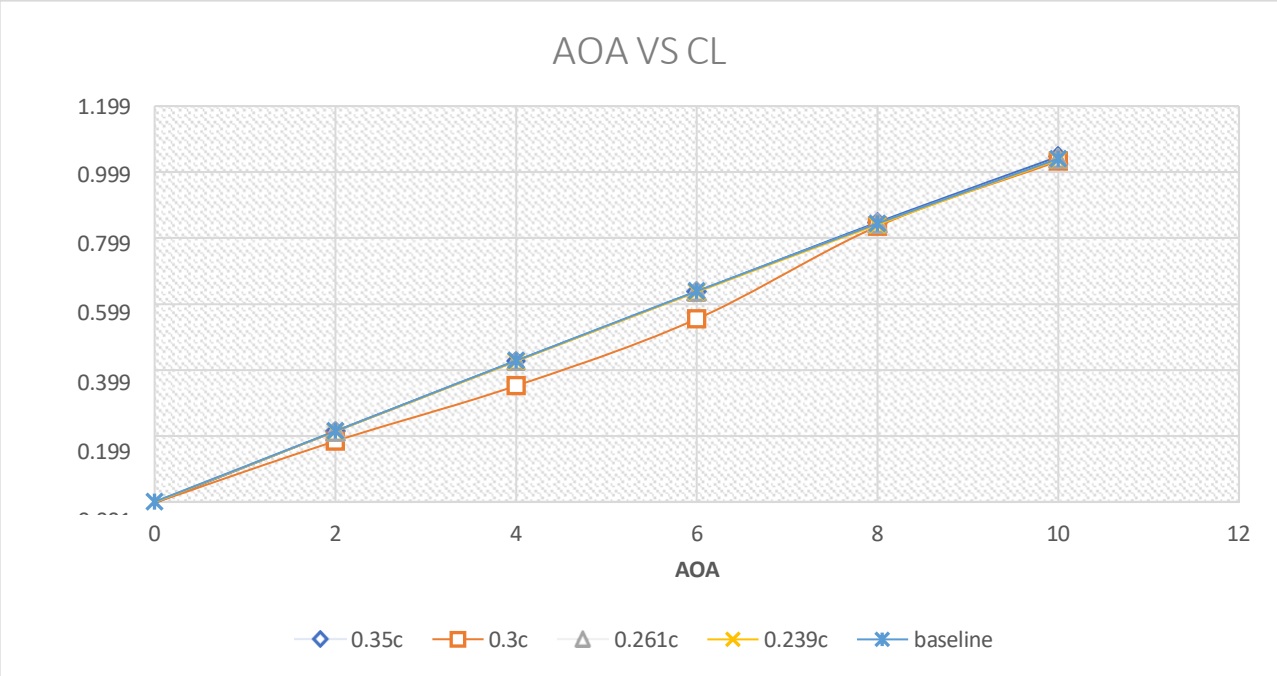

Fig. 8 *Graph angle of attack vs. lift coefficient*

Table 8 *Lift coefficient for different positions of groove*

	Lift Coefficient					
AOA	0.239c	0.261c	0.30c	0.35c	0.40c	0.45c
0	-0.00134	-0.00111	-0.00288	-0.00481	-0.00065	-0.00184
2	0.21307	0.21287	0.18363	0.21324	0.21326	0.21206
4	0.42533	0.42615	0.35119	0.42652	0.42646	0.42587
6	0.63541	0.63679	0.55376	0.63665	0.63864	0.63536
8	0.83964	0.84242	0.83457	0.84622	0.84274	0.84253
10	1.03680	1.03966	1.03234	1.04552	1.03990	1.03785

Fig. 9 and Table 9 present Cd data for different positions of the groove. Cd is minimized at 0.35c for higher AOA, reducing by up to 3% compared to baseline, indicating optimal spacing for flow control without excessive turbulence.

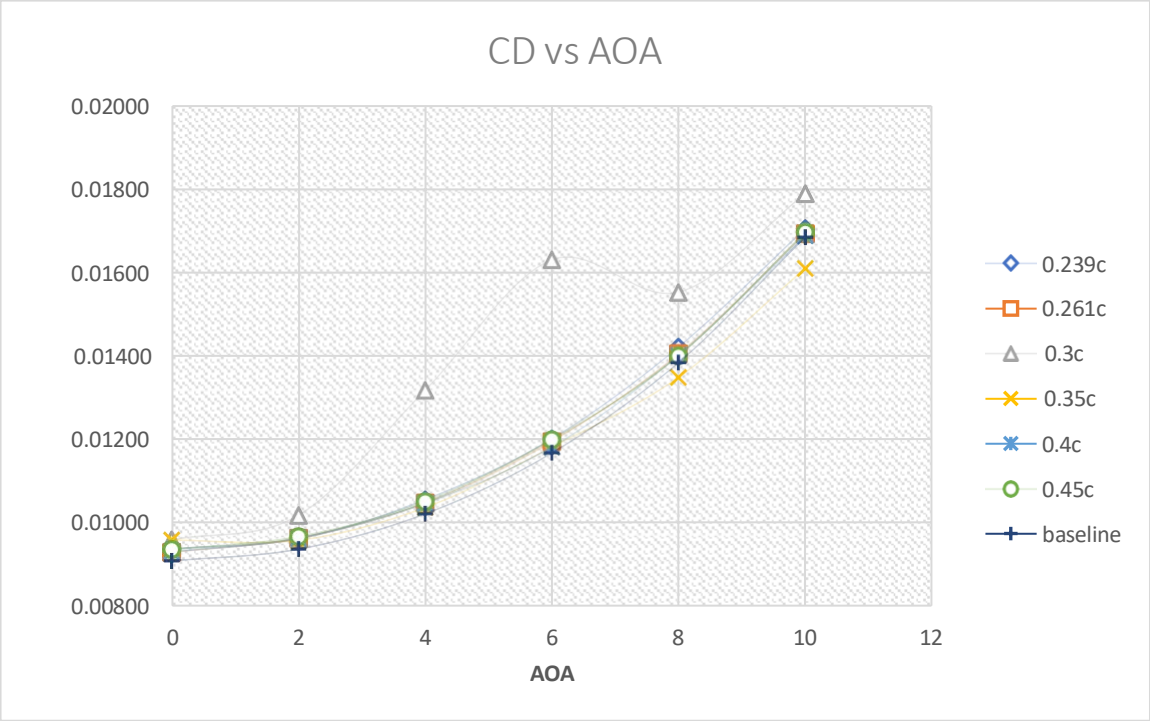

Fig. 9 *Graph angle of attack vs. drag coefficient*

Table 9 *Drag coefficient for different positions of groove*

	Drag Coefficient					
AOA	0.239c	0.261c	0.30c	0.35c	0.40c	0.45c
0	0.00937	0.00929	0.00960	0.00959	0.00931	0.00936
2	0.00962	0.00963	0.01018	0.00958	0.00963	0.00967
4	0.01056	0.01047	0.01318	0.01037	0.01046	0.01051
6	0.01201	0.01194	0.01630	0.01182	0.01182	0.01199
8	0.01421	0.01405	0.01552	0.01349	0.01401	0.01400
10	0.01705	0.01693	0.01789	0.01610	0.01688	0.01696

3.4 Analysis of the Pressure Distribution and Velocity Contour

In this section, the analysis for the pressure contour and pressure distribution for the simulation result.

3.4.1 Pressure Distribution

Fig. 10 displays the pressure coefficient (Cp) distribution at 10° AOA for the dual-groove configuration (grooves at 0.25c and 0.35c). The groove at 0.25c creates a small area of low pressure, shown by the more negative Cp values on the upper surface, which helps to create vortices that boost the boundary layer and prevent separation. This results in increased suction and higher lift, consistent with the observed Cl enhancements.

Progress in Aerospace and Aviation Technology Vol. 5 No. 1 (2025) p. 41-54

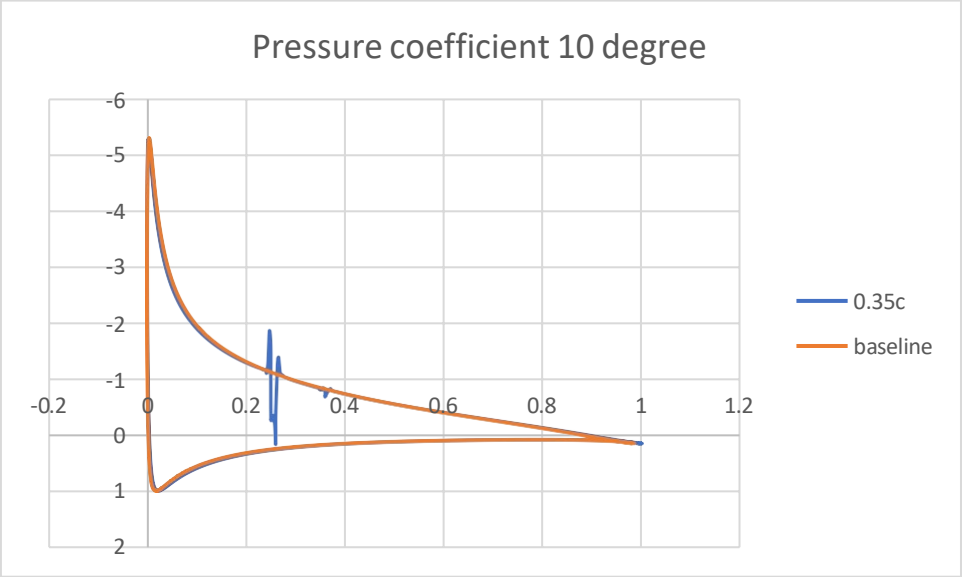

Fig. 10 *Pressure Coefficient at 10° AOA*

3.4.2 Velocity Contour

Figure 3.9 illustrates the velocity contours around the grooves for the same configuration. Within the grooves, velocities range from 0 to 10 m/s, indicating recirculation zones characteristic of vortex generators. These low-velocity regions (dark shades) suggest flow separation at the groove leading edge, with potential reattachment downstream, forming closed loops that mitigate boundary layer detachment. Per Bernoulli's principle, low velocities correlate with higher pressures at the groove base, reducing upper-surface pressure and augmenting lift. Compared to the baseline, this configuration demonstrates superior flow attachment, aligning with reduced drag post-stall [3], [4].

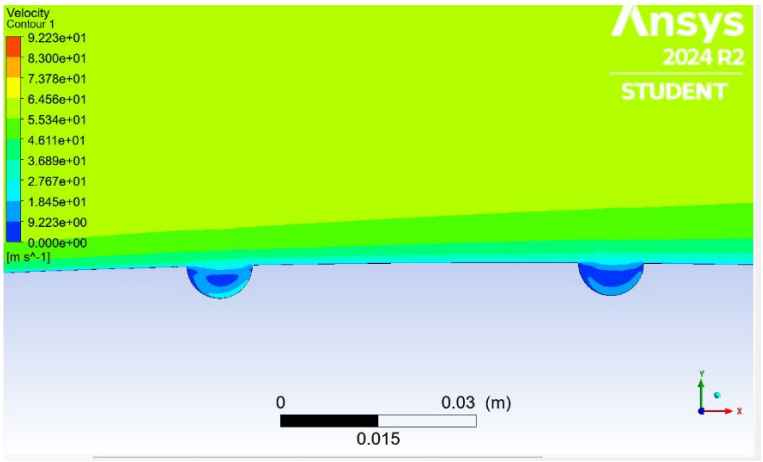

Fig. 11 *Velocity contour at the groove*

4. Conclusion

This study successfully analyzed the aerodynamic effects of semicircular grooves on the upper surface of a NACA 0012 airfoil using CFD. Validation against experimental data from Abbott and Von Doenhoff [6] showed good agreement, with simulation errors below 10%, confirming the reliability of the model. Among single-groove configurations, a groove depth of 0.01c proved most effective in delaying flow separation, increasing lift by 2–4%, and reducing drag by up to 8% at 10° AOA. Shallower or deeper grooves were less effective. For dual-groove setups (with the first groove fixed at 0.25c), placing the second groove at 0.35c provided the best overall performance, especially at higher AOAs, balancing lift improvement and drag control. Improper spacing between grooves led to reduced performance. Overall, the study confirms that semicircular grooves are a promising passive flow control method for enhancing airfoil performance at low angles of attack, with practical implications for UAV and aerodynamic design

Acknowledgement

This research was conducted with the support of the Faculty of Mechanical and Manufacturing Laboratories at Universiti Tun Hussein Onn Malaysia (UTHM). The computational resources provided by UTHM were instrumental in conducting simulations for this study.

Conflict of Interest

Authors declare that there is no conflict of interest regarding the publication of the paper.

Author Contribution

The authors confirm their contribution to the paper as follows: ***study conception and design:*** *Esmail Abdullah, Mohd Fauzi Yaakub;* ***data collection:*** *Esmail Abdullah;* ***analysis and interpretation of results:*** *Esmail Abdullah, Mohd Fauzi Yaakub, Muhammad Aideed Azman, Wan Muhammad Aqil Wan Nawang;* ***draft manuscript preparation:*** *Esmail Abdullah. All authors reviewed the results and approved the final version of the manuscript.*

References

[1] Liu, Y., Li, P., He, W., & Jiang, K. (2020). Numerical study of the effect of surface grooves on the aerodynamic performance of a NACA 4415 airfoil for small wind turbines. *Journal of Wind Engineering and Industrial Aerodynamics*, 206, Article 104263. https://doi.org/10.1016/j.jweia.2020.104263

[2] Mustak, R., Uddin, M. H., & Mashud, M. (2015). *Effect of different shaped dimples on airfoils*. Proceedings of the International Conference on Mechanical Engineering and Renewable Energy 2015 (ICMERE2015), Chittagong, Bangladesh.

[3] Chalia, S., & Bharti, M. K. (2017). Design and analysis of vortex generator and dimple over an airfoil surface to improve aircraft performance. *IJA-ERA, 3(4)*, 173-181.

[4] Srivastav, D. (2012). *Flow control over airfoils using different shaped dimples*. International Proceedings of Computer Science and Information Technology, 33, 92-97.

[5] Livya, E., Anitha, G., & Valli, P. (2015). Aerodynamic analysis of dimple effect on aircraft wing. *International Journal of Mechanical, Aerospace, Industrial, Mechatronic and Manufacturing Engineering*, 9(2), 350-353. https://doi.org/10.5281/zenodo.1099926

[6] Abbott, I. H., & Von Doenhoff, A. E. (1959). *Theory of wing sections: Including a summary of airfoil data*. Dover Publications.